This is a peer-reviewed, accepted author manuscript of the following conference paper:
Alarcón, D., Yuan, J., & Schwingshackl, C. (2022). A novel test rig for the validation of nonlinear friction contact parameters of turbine blade root joints. Paper presented at IMAC XL (40th) - 2022, Orlando, United States.

A Novel Test Rig for the Validation of Nonlinear Friction Contact Parameters of Turbine Blade Root Joints

Daniel J. Alarcón, Jie Yuan, and Christoph W. Schwingshackl

Department of Mechanical Engineering
Imperial College London
Exhibition Road, SW7 2AZ, United Kingdom

ABSTRACT
The assembly of components into a large-scale engineering system naturally leads to the presence of joints with frictional interfaces. The degree of agreement between numerical models and their experimental counterparts decreases when assemblies based in this kind of interfaces are studied due to the nonlinear dynamic behaviour that joints introduce. This is, for example, the case in turbine blade root joints. The main cause for these deviations are the friction-related nonlinear damping and stiffness effects influencing the dynamic behaviour of the assembly.

The experimental measurement of these damping effects poses a challenge due to the presence of the excitation rig itself, which can introduces significant parasitic damping in the system. A free decay measurement is consequently the ideal way to extract the nonlinear behaviour, however, the exciter must be initially in physical contact with the test fixture in order to reach the high excitation amplitudes that lead to macro-slip friction in the fixture joints.

The test setup proposed in this paper is developed for a beam on which two blade root designs have been machined at both ends (dog bone). This beam is fitted between two clamps equipped with dovetail roots and pulled into tension to simulate rotational centrifugal loading, thus creating a blade root contact joint at either end of the beam. The novel excitation method excites the beam harmonically with a rigidly connected shaker to macro-slip deflection amplitudes before decoupling from the beam to release it into free decay. This test procedure allows the contactless measurement of the variation in vibrational decay in the beam and the subsequent extraction of the resulting nonlinear frictional behaviour associated with the joints.

Keywords: blade root, nonlinear damping, friction interface, test rig, macro slip

PROJECT MOTIVATION

Traditional model updating techniques based in modal testing, in which the linearity and time-invariance of the system are mathematical assumptions [1], have reached high levels of accuracy and efficiency in the last years. As a consequence, the discrepancies observed between computational models and their experimental counterparts can now be mostly attributed to effects that escape the assumptions on which linear modal analysis is founded. Nonlinearities significantly complicate modelling and make the classical CAD/CAE-based high-fidelity approach prohibitive from a computational cost perspective [2].

The assembly of engineering structures and components into large-scale systems naturally leads to the presence of joints based on friction interfaces. These joints induce a nonlinear behaviour in the system dynamics at large vibration amplitudes and consequently have a significant influence in the system vibration response. Complex assemblies such as aircraft engines and other turbomachines present a wide range of different types of damping joints such as underplatform dampers, shrouds, blade roots, etc [3]. These joints are often designed to decrease the amplitude response of their associated components by providing the appropriate damping at large excitation amplitudes, with the aim of improving efficiency and reducing the risk of high cycle fatigue [3].

Turbomachine blade roots are of great importance in aircraft engine design, as they have significant influences on the overall system vibration response. Turbine blades are inserted into their disk via a root-slot system, which, besides making the assembly possible, allows the slippage of the blades within the fixture. This kind of contact interface creates a

hysteretic type of damping with microslip (when some parts of the contact are slipping and some parts are stuck) and macroslip (when the entire contact surface slips) regimes when the turbine is in service [4]. This behaviour can be studied experimentally in a rotating rig, where the load in the root is introduced by centrifugal forces. A rotating rig is however very complex and expensive to build, operate and instrument. Exciting the blade and its associated root to cause macroslip friction in the joint is particularly challenging since large forces are needed to excite the system to operating conditions. Solutions such as excitation by means of air jets [5] or alternating magnets [6] have been implemented by researchers in this field, but generally very low amplitudes are achieved on the tested blades.

Alternatively static rigs have been used, where the centrifugal forces are replaced by pulling forces [4, 7]. The advantages related to the use of a static rig for this study are manifold. The rig excitation can be controlled more accurately at a fraction of the design and operating costs of a rotating rig, a single trained operator can be in charge of the entire rig, and changes in the design and construction of the rig can be implemented in a straightforward manner. On the other hand, rig designs tend to become overcomplicated by trying to isolate the specimen from rigid body rig resonances and parasitic damping. Operational challenges related to loss of load in the specimen over time, material creep/plastic deformation, and the inability of the rig to hold shear forces related to the dynamic excitation of the specimen may arise as well.

Nevertheless, the main challenge posed by static rigs lies in the excitation system. In order to cause macroslip friction in the joints, large deflection amplitudes must be excited. This can only be effectively achieved by using a traditional electrodynamic shaker. Schwingshackl et al. [3] found that attaching the shaker permanently to the specimen would yield the required excitation levels, but the excitation fixture itself added parasitic damping to the rig. Instead, detaching the excitation fixture from the bone after a running-in phase would yield satisfactory results with very little added parasitic damping but the chosen mechanism would not reach the required amplitudes.

The authors propose in this work a novel excitation fixture for the Dogbone Test Rig, capable of both evenly pulling and pushing the bone with a stable shaker connection and then cleanly detaching the excitation system once the required amplitudes are reached. Detaching the excitation fixture, namely the shaker and its pushrod, allows the free vibrational decay measurement of the bone without the impact of the shaker and in consequence an extraction of amplitude-dependent damping via the piecewise logarithmic decay equation (Figure 1) [3].

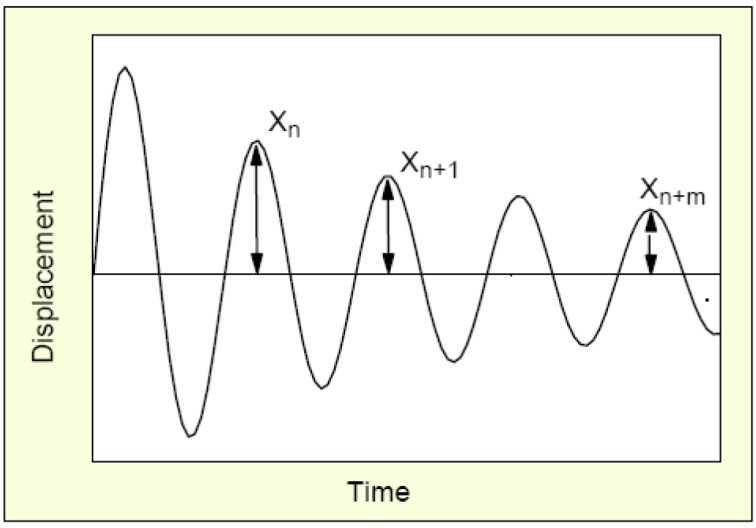

Figure 1: Logarithmic decay method to calculate the logarithmic decrement δ [3].

$$\delta = \frac{1}{m} \ln \frac{x_n}{x_{n+m}}$$

$$\zeta = \frac{1}{\sqrt{1 + \left(\frac{2\pi}{\delta}\right)^2}}$$

In these equations and in Figure 1, m is the number of peaks for which the logarithmic decrement is calculated for. x_n refers to the point in the x axis where the calculation starts, namely, the highest peak; and x_{n+m} is the last point for which the logarithmic decay is calculated. In the results and discussion chapter of this paper m is always 1, as the logarithmic

decay is calculated in a peak-to-peak basis. ζ is the damping ratio, a non-dimensional characterization of the decay rate relative to the frequency.

THE DOGBONE TEST RIG

The test setup presented in this paper is an evolution of a concept first introduced by Allara et al. [8]. This is known as a "dog bone" setup (Figure 2), which has a beam with a rectangular cross-section as its central component. Two blade roots have been machined at either end of this beam, which enables its attachment to two compatible roots machined into the edge of a solid disc. These discs are pulled apart to simulate a centrifugal load while a harmonic excitation load is applied to excite a particular mode shape in the bone. Both joints behave in consequence as a blade root joint. This concept was implemented by Marquina et al. [7] and by Schwingshackl et al. [3] in the past.

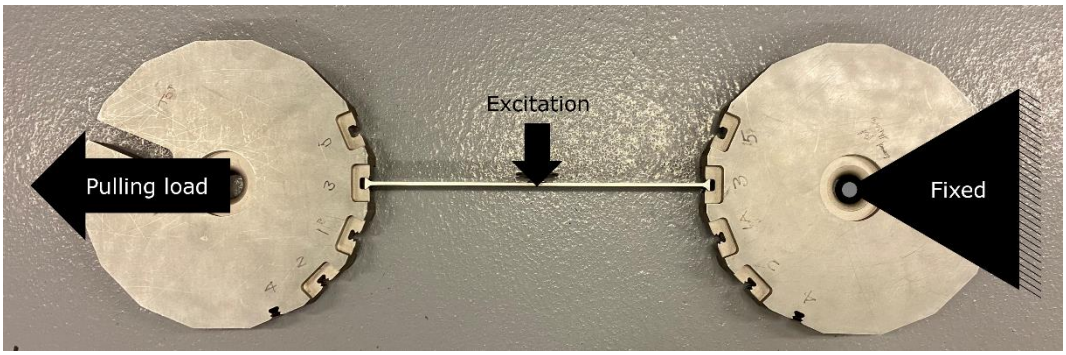

Figure 2: Schematics of a dog bone setup for the study of blade root contacts.

The centre of these discs has a hardened bore with rounded edges, which allows sliding a U-shaped shackle through the bore as Figure 3a shows. Each shackle is trapped in the grips of an electromechanical tensile/compressive test machine (Instron 5980, Figure 3a), capable of loads of up to 250 kN with a gripping pressure of 6 bar. The entire dog bone assembly is loaded by moving the upper crossbar a few tenths of a millimetre to a nominal loading of 2.2 kN. This creates two blade root friction contacts at either end of the beam as shown in Figure 3b.

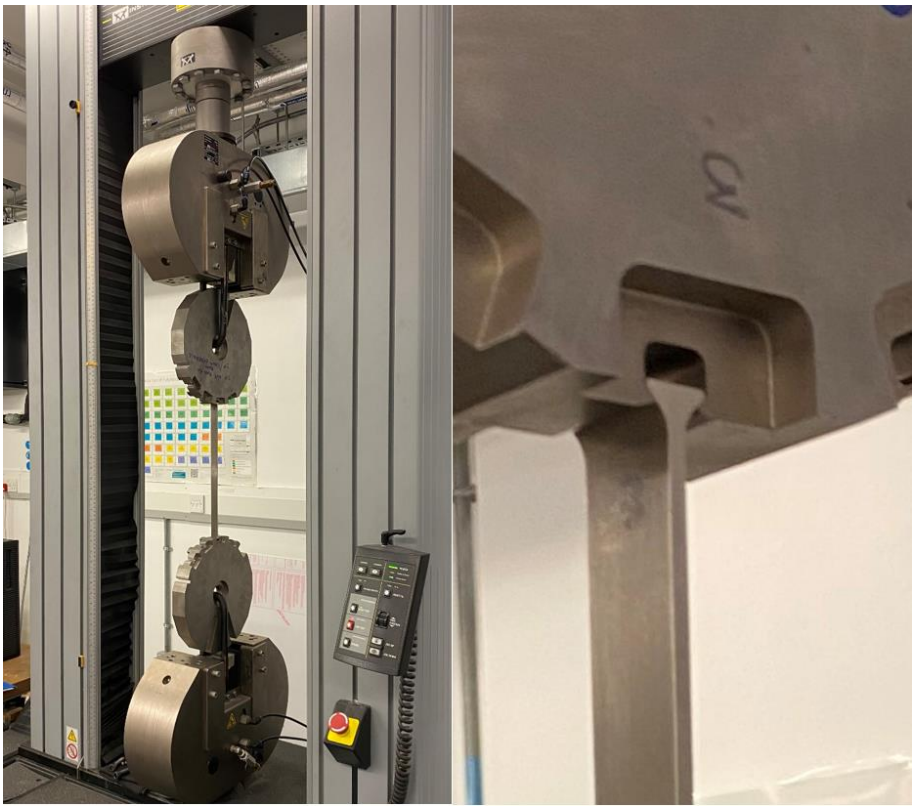

Figure 3: a) Dog bone assembly under load in the Instron 250 kN tensile/compressive machine. b) Detail view of the upper root contact. The lower contact is analogous.

This arrangement allows, as proven in [3], to minimise the parasitic damping introduced by the supporting structure. The main difference between the current dog bone setup and the one in [3, 7] is that the current bone is shorter and thinner, measuring 315 mm in length and with a rectangular cross-section of 18x3 mm, made of AISI 316 stainless steel. The shorter length allows to mount the dog bone assembly in the more compact tensile/compressive machine, thereby increasing the versatility of this rig.

A NOVEL EXCITATION METHODOLOGY

The main idea of this excitation mechanism consists of a power-to-release electromagnet that couples the bone rigidly to the shaker during the excitation. The magnet can be released at any point during a vibration cycle, decoupling this way the shaker from the bone (Figure 4). An offset introduced to the shaker, and triggered at the same time as the magnet release, ensures that the magnet is pulled away from the bone. A power-to-hold electromagnet behind the shaker is used to hold the shaker back from its excitation position during the release action. This magnet ensures that the pushrod assembly does not impact the bone after a release.

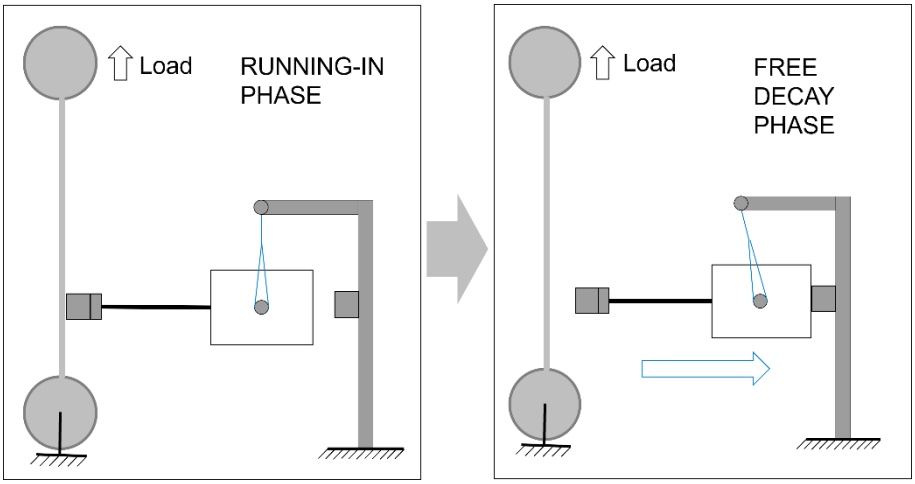

Figure 4: Graphical representation of the working principle of this excitation fixture.

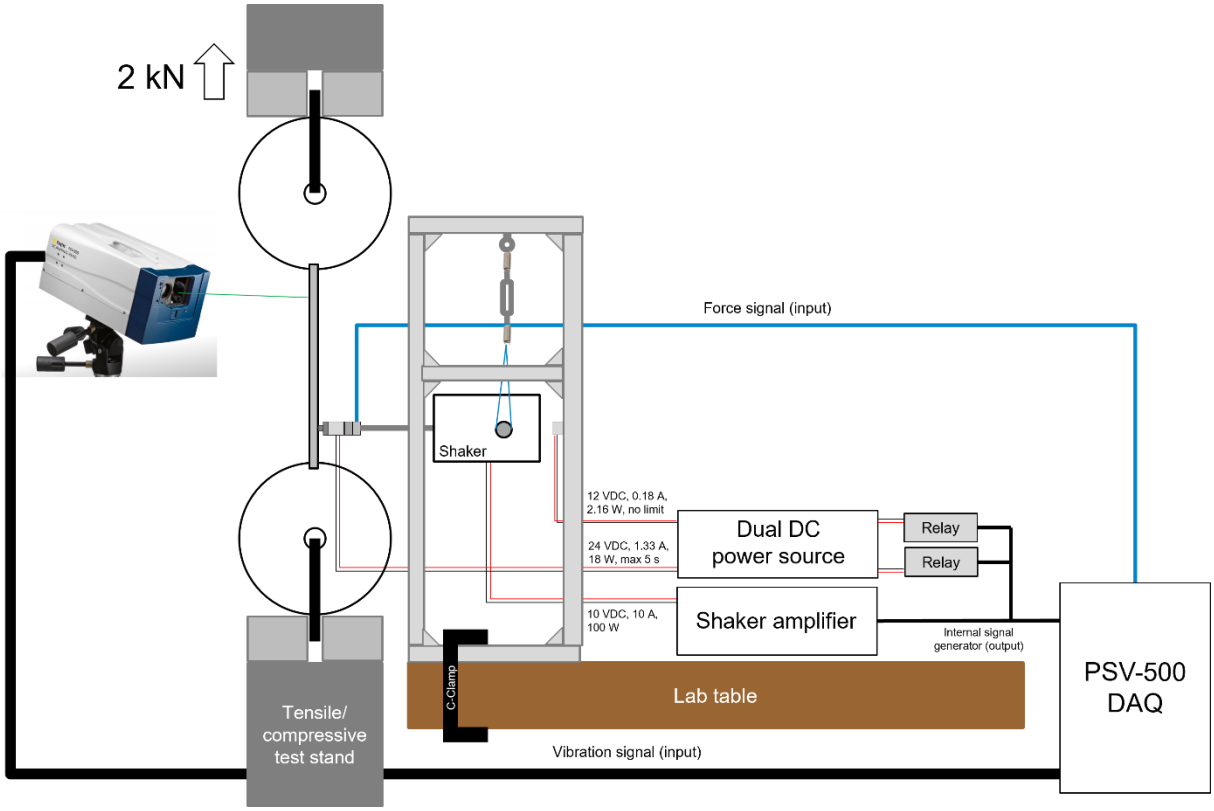

Figure 5: Scheme of the Dogbone Test Rig with its excitation fixture, measurement and data acquisition system as of October 2021.

A schematic representation of technical implementation of the excitation fixture on the Dogbone Test Rig is shown in Figure 5. The shaker assembly is represented attached to the bone for illustrative purposes.

The excitation is provided by an electrodynamic shaker (Data Physics GW-V20) connected to a PA300E amplifier than can deliver up to 100 N of excitation force. The shaker hangs off a 40x40 mm aluminium struts frame equipped with stiff springs and turnbuckles to easily regulate the shaker height according to the experimental requirements. The frame is clamped to a laboratory table by means of four C-clamps.

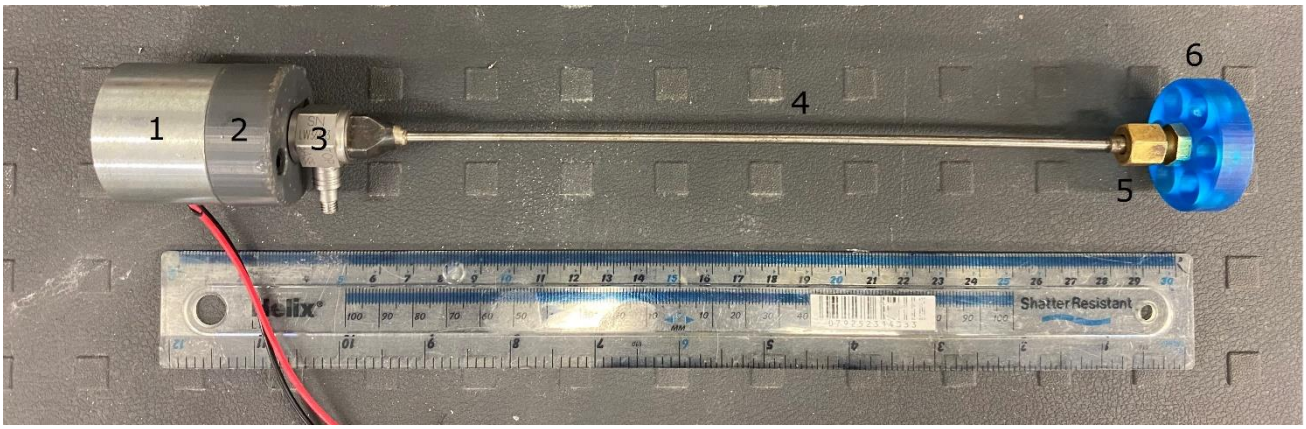

Figure 6: Pushrod assembly (ruler for scale) with numbered main components.

The shaker is equipped with a pushrod assembly (Figure 6) with an array of components screwed to one another. Component number 1 in the figure is a 40x30 mm power-to-release electromagnet (Bunting XH4030) with a load capacity of 160 N. Two M4 drillings in the electromagnet's casing allow screwing it to an interface part (part 2) 3D printed of Formlabs Tough 2000 resin. The other side of this interfacing part is equipped with an M6 hole to attach a quartz piezoelectric force sensor (PCB 208C02 (3)) by means of an adapting stud. The force sensor is directly screwed to a custom-built pushrod (4) with a 10-32 UNF mounting stud. The opposite end of the pushrod presents a rounded contact for an easy alignment and mounting of the shaker, and is finished on a female brass connector (5). This connector is compatible with a male brass connector attached to another 3D printed part (6) made of blue Formlabs Tough V5 resin. This printed part allows screwing the pushrod assembly to all seven mounting holes on the shaker armature, and to minimize operational strain on the central armature screw.

Current is supplied to both electromagnets by a dual DC power source, which simultaneously supplies 24 VDC, 1.33 A to the power-to-release magnet and 12 VDC, 0.18 A to the power-to-hold electromagnet. Two solid-state relays (Schneider Electric 70S2(S)) close the power circuit that supplies the magnets when they detect a DC voltage higher than 3 V. This trigger signal is supplied by the user-defined signal generator built in the Polytec PSV-500 data acquisition card (DAQ) together with the excitation signal for the shaker. The signal generator is connected to both relays and to the shaker amplifier; this solution controls the circuit action and the shaker with one fully customizable single input signal.

The excitation and relay trigger signal (Figure 7), based in the work of Mace et al. [10], has an absolute amplitude of 10 VDC, which is the maximum voltage supplied by the PSV-500 DAQ, and has three stages: I) A sinusoidal waveform of amplitude +/− 1 VDC is supplied at the frequency of interest to excite the bone for 10 seconds; II) A steep ramp is then added to the excitation signal to pull the shaker back from the bone. This ramp is used as well to trigger the relays to close the power circuit, and thus feeding the magnets. The power-to-release electromagnet demagnetizes approximately at the same time as the shaker starts pulling back leading to a release of the bone and the removal of the excitation system. III) A sinusoidal waveform to keep some vibration in the shaker during the free decay of the bone for another 5 seconds. The shaker and pushrod assembly stays retracted for about 5 seconds, which is close to the maximum feeding time the power-to-release electromagnet can safely hold. After this, the power is cut from the electromagnets and the shaker attaches back to the bone, returning the setup to its original state.

The vibrational response from the bone is measured with a Polytec scanning laser Doppler vibrometer (LDV) head connected to the PSV-500 DAQ. This upgraded model of scanning head does not require any prior surface treatment or the application of retroreflective adhesives on the bone due to its use of an infrared laser. Data is sampled with

2.5 kSamples for a bandwidth of 1 kHz discretized with 12800 Fast Fourier Transformation (FFT) lines. This results in a measured time block of 12.8 s and a resolution of 0.1 Hz.

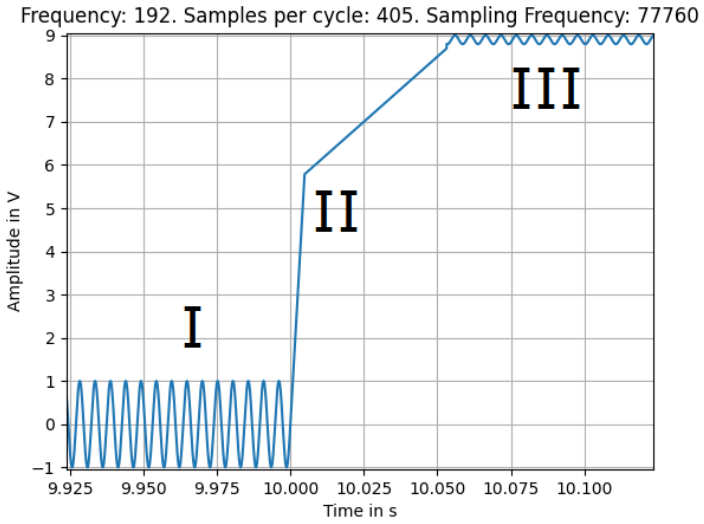

Figure 7: Sample of a signal fed to the electrodynamic shaker and the relays with three numbered stages.

RESULTS AND DISCUSSION

The current Dogbone Test Rig concept, where the pushrod and the shaker retract from a specimen due to the action of two electromagnets, was investigated on a proof-of-concept rig before its full-scale implementation (Figure 8). Two heavy steel L-profiles were clamped to a laboratory bench, and a steel bar measuring 300x50x5 mm was rigidly clamped to each of these profiles. This bar was first swept with a stepped sine sweep between 50 and 500 Hz to find the first natural frequency of bar and shaker at 138 Hz.

Figure 8: Proof-of-concept implementation of the Dogbone Test Rig on a double clamped stiff test specimen.

A test campaign was carried out to study the influence of different variables in the release, for example, the phase angle at which the offset ramp starts, the shaker boundary conditions, etc.

The influence of the shaker and magnet trigger signal was studied and the signal was made more adaptable by adding two phase parameters. A phase multiplier parameter makes possible starting the offset ramp at angles 0, π/2, π or 3π/2 rad (Figure 9). A phase tuning parameter, taking in values of 0, π/8, π/4 or 3π/8 rad contributes to a further fine-tuning of the phase angle at which the offset ramp starts.

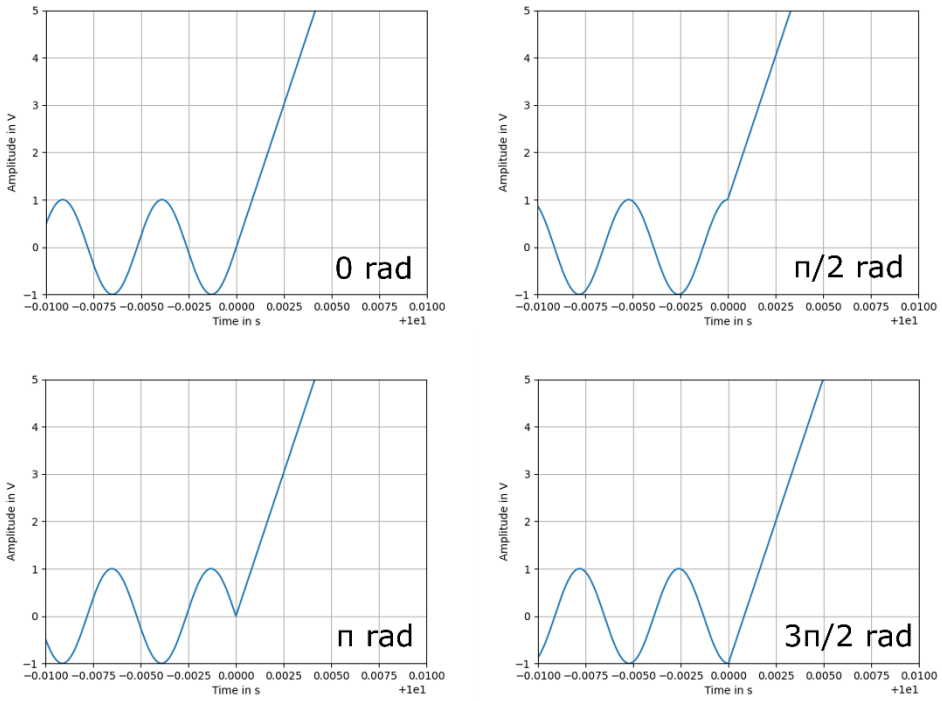

Figure 9: Effect of different phase multiplier values in the offset ramp start.

The shaker release was studied under three different boundary conditions: 1) with the shaker mounted on its base and simply resting on a laboratory bench, 2) with the shaker mounted on its base and resting on two steel cylinders (which allowed the movement of the shaker in the axial direction); and 3) with the shaker hanging from two pillars as Figure 8 shows. It was found that hanging the shaker yielded notably cleaner releases on the proof-of-concept rig (Figure 10). The hanging setup was still stiff, but nevertheless it successfully decoupled the shaker from the assembly.

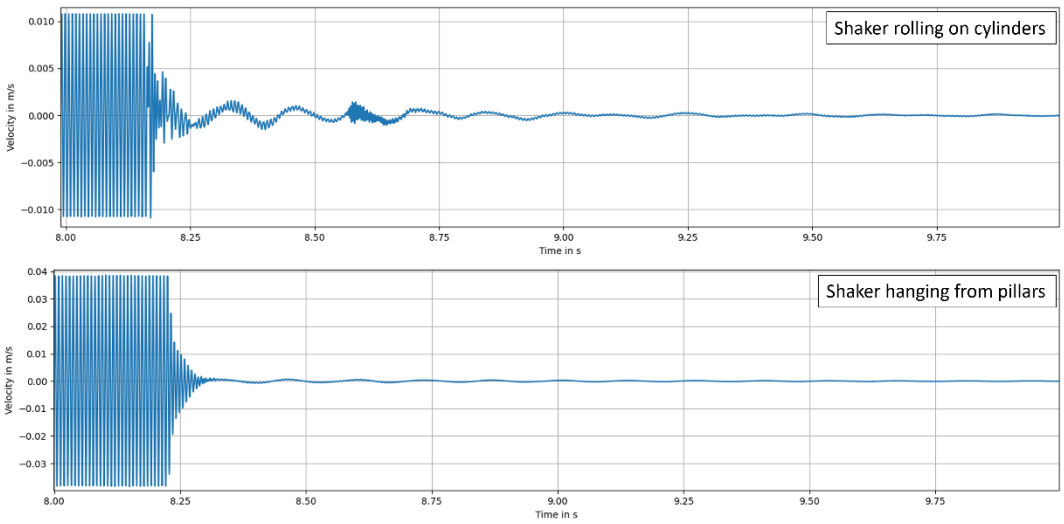

Figure 10: Top − Velocity signal measured after releasing the double clamped beam from the shaker mounted on its base and rolling on cylinders. Bottom – Velocity signal measured after releasing the double clamped beam from the hanging shaker.

The measured response signals required some of postprocessing. Firstly, given that the Dogbone Test Rig pursues the measurement of damping as a function of vibrational amplitude, the velocity signal measured by the LDV must be integrated to have a displacement signal. This tends to amplify the signals' low-frequency components. The measured

response was windowed with a tapered Hanning window (also known as a Tukey window or cosine-tapered window) with an alpha parameter of 0.1. In essence, this window attempts to smoothly set the data to zero at the boundaries of the signal while not significantly reducing the processing gain of the windowed transform [10]. A bandpass filter with order 5 between 80 and 200 Hz is also applied as Figure 11 shows. This is necessary to remove the very low frequency vibration in the proof-of-concept rig caused by the laboratory bench, which is not rigidly attached to the floor, and to remove higher order harmonics in the specimen.

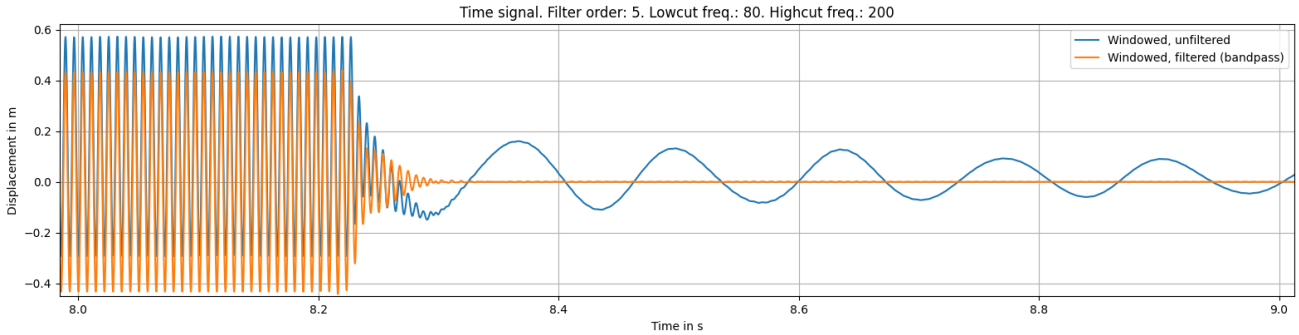

Figure 11: Freely decaying signal measured after detaching the shaker from the test specimen on the proof-of-concept rig. In blue, the unfiltered displacement signal. In orange, the filtered displacement signal.

A peak-to-peak envelope of this decaying signal is calculated (Figure 12a) using a free-domain Python implementation by Bergman [11] of the MATLAB `peakdet` code created by Billauer [12]. This code requires controlling for the so-called look ahead value and the delta value. The look ahead value is the distance to look ahead from a peak candidate to determine if it is the actual peak, and is set to 1 after some trial and error (a value of 1.25 is suggested in [12]), and the delta is kept at a default value of 0. Each pair of consecutive envelope points is used in the calculation of the logarithmic decay with the equations in the project motivation section. Figure 12b, shows the calculated damping ratio ζ for each point plotted against the vibration amplitude. Little variation of the damping ratio against the vibration amplitude was expected as the specimen used for this proof-of-concept rig is made of structural steel and is rigidly double clamped to the test fixture. However, the data points below 1 in Figure 12b, are related to a sudden change in the decrement of the envelope function observable in Figure 12a at a displacement amplitude of about 0.12-0.14 mm.

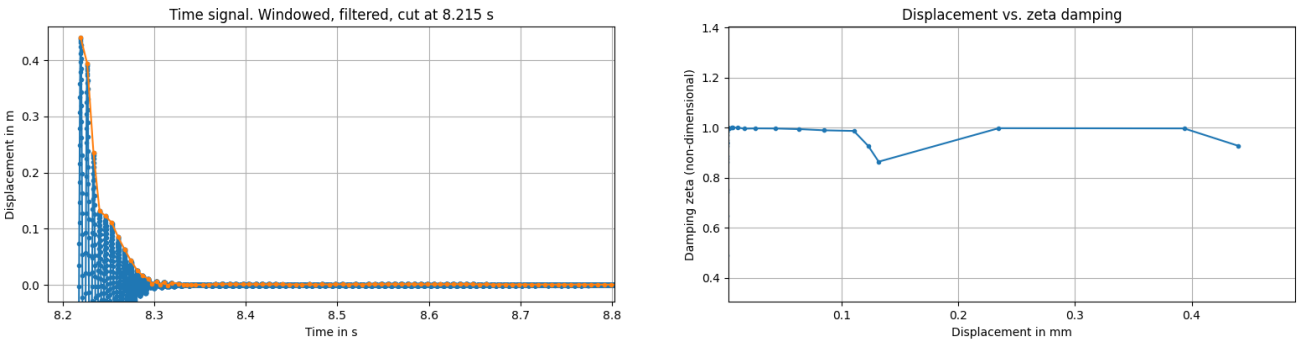

Figure 12: a) Envelope of the decaying signal in orange, decaying signal plotted in blue. b) Amplitude (displacement) plotted versus the damping ratio ζ.

It was felt at this stage that the approach proven in the proof-of-concept rig could be transitioned to the full-scale Dogbone Test Rig. Figure 13 shows an initial implementation of the excitation fixture. An extra fixture to keep the pushrod from dropping after releasing was installed (Figure 14) after a few initial trials. Figure 14 shows as well a small structural steel interfacing part between bone and power-to-release electromagnet. The construction material of the bone (AISI 316 stainless steel) is non-magnetic and therefore, the attachment of this interfacing part is necessary to make the setup work. The interface part is glued to the bone with Loctite 495 adhesive. Screwing both parts would have required drilling the bone, which would create a stress concentration point, decreasing thus the safety factor of the design. A bone built of magnetic AISI 430 stainless steel is being currently manufactured, which will render this interfacing part unnecessary in the future.

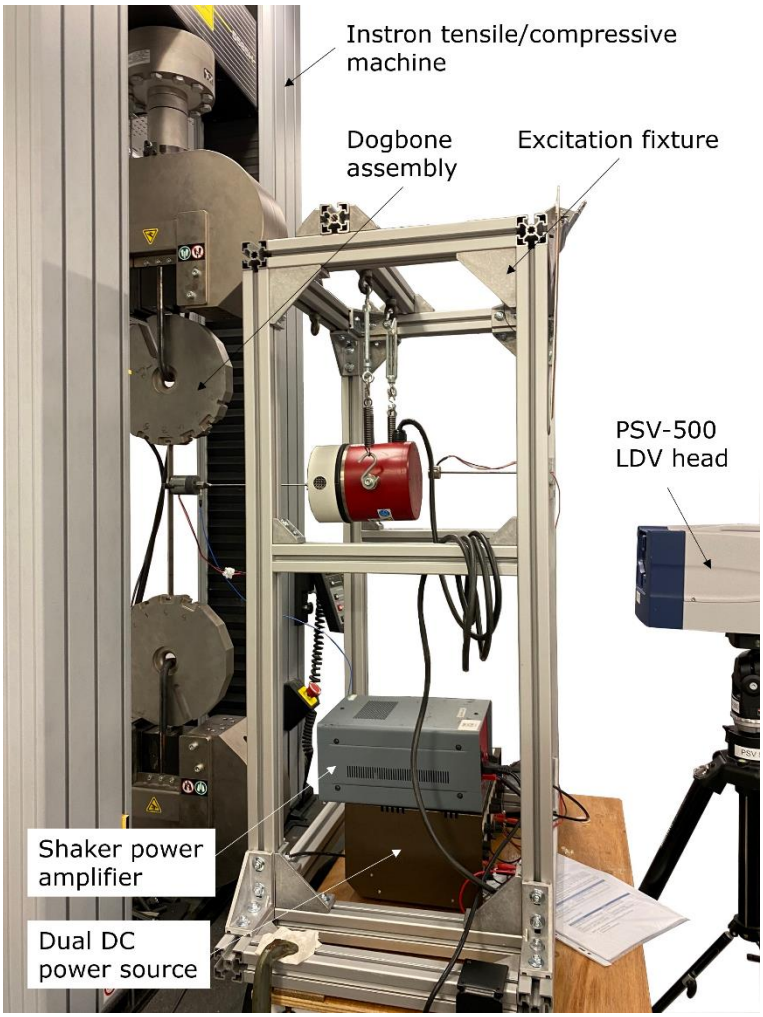

Figure 13: Full-scale Dogbone Test Rig with the bone assembly mounted with a load of 2.2 kN on the Instron 250 kN tensile/compressive test stand, shaker amplifier, dual DC power source and the PSV-500 SLDV head.

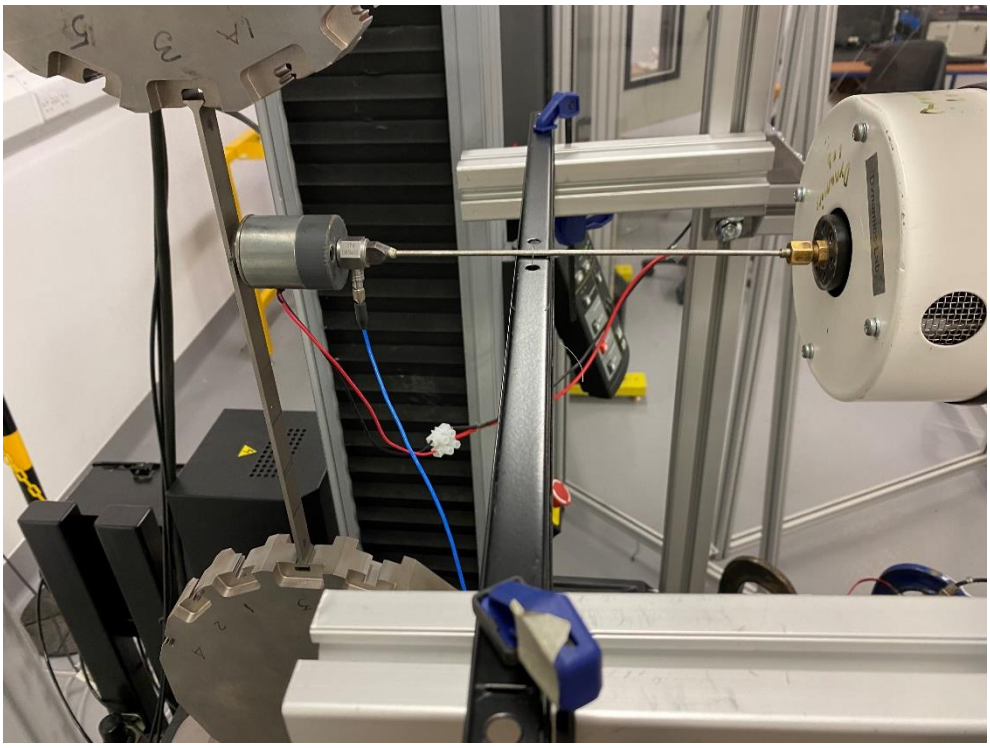

Figure 14: Extra fixture installed added to the frame to hold the pushrod from falling after a release.

A resonance test was firstly conducted by means of a handheld modal hammer (PCB 086C02) and the PSV-500 on the bone and its root discs to rule out any influences of the rig in the resonance frequencies of the bone. Figure 15 shows an overlay of all Frequency Response Functions (FRFs) measured in the test. The low frequency peaks of these FRFs are related to out of plane rigid body motion of the bone and rotation motion in the root discs, while the peaks around 192 Hz and beyond are flexible bone modes. The FRFs that do not present peaks beyond the 30 Hz range are FRFs measured on the root discs. Consequently, there seems to be no significant flexible deflection at the discs, highlighting the decoupling of rig from the bone.

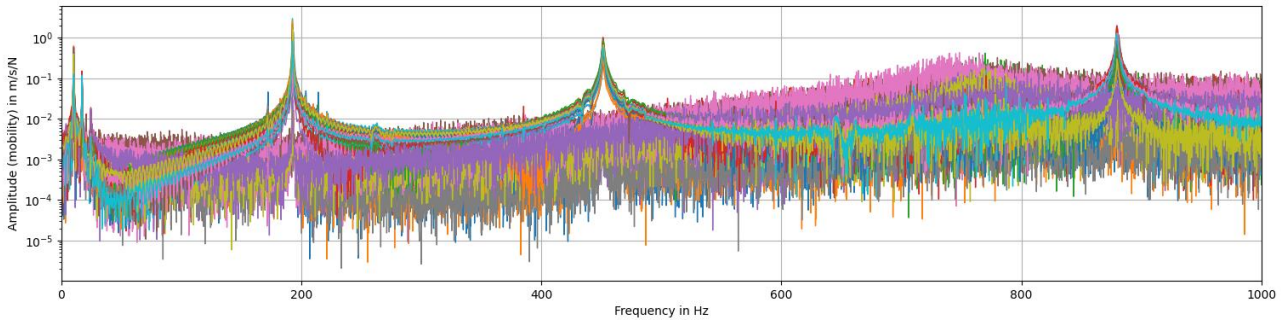

Figure 15: Overlay of all Frequency Response Functions (FRFs) measured in the resonance test.

The release mechanism proven in the proof-of-concept rig was then employed after loading the bone to 2.2 kN and exciting it with an excitation force of 40 N, but unfortunately the first tests on the full-scale Dogbone Test Rig did not yield the same quality of release results as the proof-of-concept rig did. At the moment of writing this paper, all datasets present an extremely high-amplitude low-frequency vibration of about 9 Hz after release due to the rigid body rotation of the two discs, which makes a decent extraction of the free decay damping rather challenging (Figure 12, plotted in blue). A high-pass filter set at 30 Hz would remove this undesired frequency (Figure 16, plotted in orange), but this is, however, not ideal since the target is to work on an unfiltered data set. Even though the low-frequency component could be filtered out, most of the vibration in the root contact will still be dissipated by friction damping related to this low frequency vibration, not by the first flexible mode of the bone.

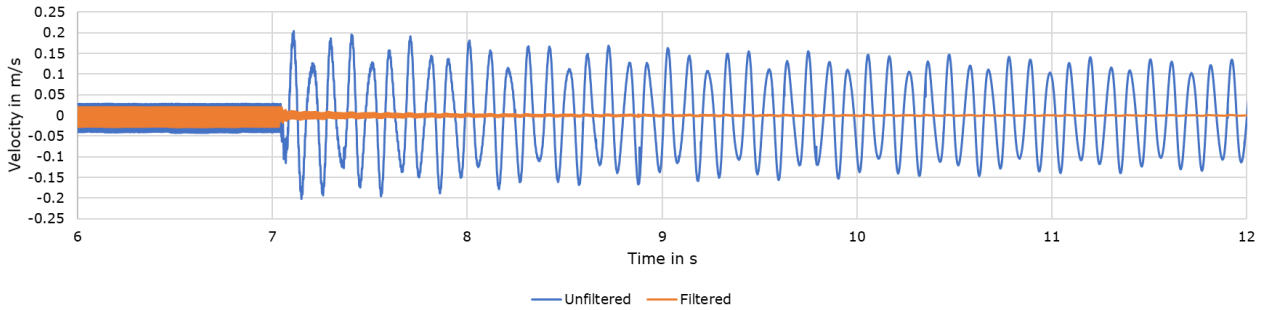

Figure 16: Overlay of the response in the full-scale Dogbone Test Rig after an unsuccessful release (blue) and the same signal with a high-pass filter at 30 Hz (orange).

FURTHER WORK

The authors are currently striving to solve this issue in order to obtain clean releases from the full-scale rig. It is hypothesized that the retracting action from the shaker and the disengagement of the power-to-release magnet do not happen in a synchronous manner, but there is a small delay in the magnet action. While this issue seemed to be overcome by the larger stiffness of the system in the proof-of-concept test rig, the Dogbone Test Rig is too flexible to operate in this way and the bone experiences a strong pull as the shaker is pulled backwards while the power-to-release magnet is still engaged during this time lapse. The relays have, according to their datasheet [13], a control voltage range of 3-15 VDC. Therefore, they will close the circuit when triggered with 3 VDC or higher. With the current ramp gradient shown in Figure 17, this happens at $\Delta t = 0.0024$ s after an offset ramp starts. A lapse of approximately 0.002 can be as well observed in the time signals measured in unsuccessful releases.

The relays datasheet also specifies a maximum relay turn-on time of 75 ms [13], which is represented by the area shaded in red in Figure 14. This time lapse would encompass the entire offset ramp and the release would take case, in a worst

case scenario, when the shaker has already pulled back from the bone. This accumulated delay does not take into account the demagnetizing action delay of the electromagnet, which cannot be found specified in any datasheet.

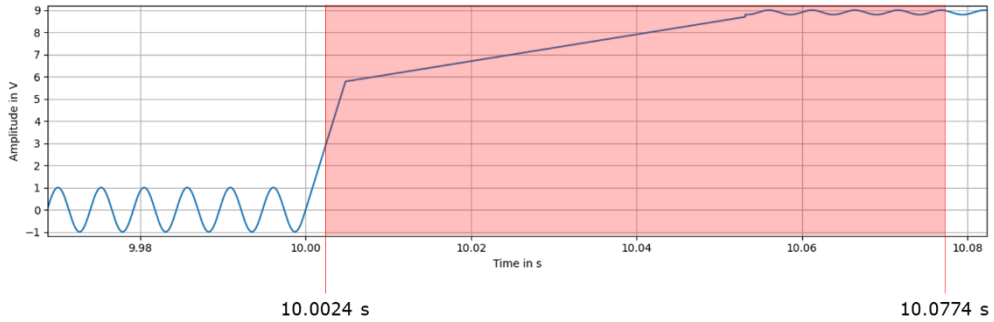

Figure 17: Plot of the signal fed to the electrodynamic shaker and the relays with timestamps at the 3 VDC threshold and the relays' specified maximum turn-on time.

To address this potential release delays, it is necessary to make changes in the way the shaker pullback and the relays are triggered. Shaker and relays must receive signals independent from each other. This cannot be achieved with the DAQ built in the PSV-500 to the authors' knowledge, as only a single user-defined signal generator is available in the software in its current version. Currently a new setup is being implemented with an external National Instruments cDAQ-9188 equipped with a NI 9263 analog output module. In this way the excitation and offset signal and the relay trigger signal can be sent independently, with the shaker ramp starting at a time t, while an independent voltage step signal is sent to the relays earlier to close the power circuit at a time Δt, which is now an adjustable interval. Finding the appropriate gap between relay activation and offset ramp start will be a matter of trial and error if the maximum relay turn-on time and the unspecified magnet demagnetization time are taken into account.

CONCLUSIONS

The Dogbone Test Rig presented in this work is a solution to study the amplitude-dependent, frictional behaviour associated to turbine blade root joints. It tries to overcome the shortcomings that similar setups presented in past investigations, particularly the excitation of the root to representative amplitudes. The innovation in the experimental setup lies in the use of power-to-release and classical electromagnets to detach the electrodynamic shaker and pushrod from the bone after reaching steady-state high frequency vibration and to allow the test specimen to freely vibrate. This work has described the complexity of such a rig, which is composed of different components working together simultaneously. Initial tests showed a clean release with the proposed system, but currently more work is underway to adapt the setup for the actual full-scale test rig.

ACKNOWLEDGEMENTS

The work in this paper is part of a work package in the project Systems Science-based Design and Manufacturing of Dynamic Materials and Structures (SYSDYMATS), funded by the Engineering and Physicals Sciences Research Council with grant reference EP/R032793/1.

REFERENCES

[1] Ewins, D.J., *Modal Testing: Theory and Practice*, p. 95, 5th ed., John Wiley & Sons, Chichester, UK

[2] Yuan, J., Schwingshackl, C.W., Wong, C., Salles, L., "On an improved adaptive reduced-order model for the computation of steady-state vibrations in large-scale non-conservative systems with friction joints", *Nonlinear Dynamics* 103, 3283-2200, 2021

[3] Schwingshackl, C.W., Joannin, C., Pesaresi, L., Green, J.S., Hoffmann, N., "Test method development for nonlinear damping extraction of dovetail joints", *Dynamics of Coupled Structures, Vol. 1*, Conference Proceedings of the Society for Experimental Mechanics Series, pp. 229-237, 2014

[4] Schwingshackl, C.W., Zolfi, F., Ewins, D.J., Coro, A., Alonso, R., "Nonlinear friction damping measurements over a wide range of amplitudes", *Proceedings of the IMAC-XXVII,* Orlando, FL, February 9-12, 2009

[5] Kurstak, E., D'Souza, K., An Experimental and Computational Investigation of a pulsed Air-jet Excitation System on a Rotating Bladed Disk, *Proceedings of the ASME Turbo Expo 2020*, September 21-25, 2020

[6] Kruse, M.J., Pierre, C., An Experimental Investigation of Vibration Localization in Bladed Disks, Part I: Free Response, Proceedings of the International Gas Turbine & Aeroengine Congress & Exhibition, Orlando, FL, June 2-5, 1997

[7] Marquina, F.J., Coro, A., Gutiérrez, A., Alonso, R., "Friction Damping Modelization in High Stress Contact Areas Using Microslip Friction Model", *Proceedings of GT2008 ASME Turbo Expo 2008: Power for Land, Sea and Air*, Berlin, Germany, June 9-13, 2008

[8] Allara, M., Filippi, S., Gola, M.M., "An Experimental Method for the Measurement of Blade-Root Damping, *Proceedings of the ASME Turbo Expo*, Barcelona, Spain, May 2006

[9] Mace, T., Taylor, J., Schwingshackl, C.W., "A Novel Technique to Extract the Modal Damping Properties of a Thin Blade", *Topics in Modal Analysis, Vol. 8*, Conference Proceedings of the Society for Experimental Mecanics Series, pp. 247-250, 2019

[10] Harris, F.J., On the Use of Windows for Harmonic Analysis with the Discrete Fourier Transformation, *Proceedings of the IEEE*, Vol. 66, No. 1, January 1978

[11] Bergman, S., peakdetect [Online], Available: https://pypi.org/project/peakdetect/1.1/, retrieved October 2021.

[12] Billauer, E., peakdet: Peak detection using MATLAB [Online], Available: http://billauer.co.il/peakdet.html, retrieved October 2021.

[13] Schneider Electric USA, Inc., *Legacy Schneider Electric Solid-State Relays – Catalog 2017*, p. 20, version 06/2017